applied sciences

MDPI

Article

Optimization Design of the Mix Ratio of a Nano-TiO_2/$CaCO_3$-Basalt Fiber Composite Modified Asphalt Mixture Based on Response Surface Methodology

Yafeng Gong, Jiaxiang Song, Haipeng Bi * and Zhenhong Tian

College of Transportation, Jilin University, Changchun 130025, China; gongyf@jlu.edu.cn (Y.G.); songjx18@mails.jlu.edu.cn (J.S.); tianzh17@mails.jlu.edu.cn (Z.T.)

* Correspondence: bihp@jlu.edu.cn; Tel.: +86-155-8410-0916

Received: 11 June 2020; Accepted: 29 June 2020; Published: 2 July 2020

Abstract: This research optimizes the mix ratio of nano-TiO_2/$CaCO_3$ (NTC)-basalt fiber (BF) composite modified asphalt mixture. Based on the Box–Behnken method and the response surface method, a three-factor and three-level test was designed. The input indicators were the asphalt–aggregate ratio, NTC content, and BF content. The output indicators were the density, air voids, Marshall stability, flow value, voids in mineral aggregate (VMA), and voids filled with asphalt (VFA) values of the asphalt mixture. The response surface model was established according to the test response index value. Then, the function was fitted through multiple regression equations and multivariate analysis of variance was performed. Finally, according to the specification requirements and engineering needs, the selected conditions of each response value were determined to optimize the asphalt–aggregate ratio and the contents of NTC and BF, and the predicted values were verified through the measured data. The test results show that the optimal contents of NTC and BF and the optimal asphalt–aggregate ratio were 5.1%, 3.9%, and 5.67%, respectively. By comparing the measured Marshall test index value with the predicted value, the minimum relative error was 0.096% and the maximum error was 6.960%. The results show that response surface methodology can be used to optimize the mix ratio of composite modified asphalt mixtures.

Keywords: response surface methodology; nano-TiO_2/$CaCO_3$; basalt fiber; composite modified asphalt mixture

1. Introduction

In recent years, with the increase of traffic flow and the deterioration of the environment, it is becoming increasingly difficult for existing asphalt pavement to meet requirements, meaning modified asphalt technology is very important. Improving the durability and stability of pavement through modification of asphalt is a new challenge [1]. With the emergence of nano-modified and fiber-modified asphalts, the performance of asphalt pavement has been effectively improved, and the service life of asphalt pavement has also been improved.

Due to the large specific surface area of the nanomaterials, after being added to the asphalt, the nanomaterials can improve the cohesion and also increase the viscosity and high temperature stability of the asphalt, thereby improving the high temperature performance and water stability of the asphalt mixture. Chang et al. [2] added different proportions of nanometer calcium carbonate to SBS (styrene–butatriene–styrene) modified asphalt and analyzed the high- and low-temperature stability of the composite modified asphalt via changes of the nanometer calcium carbonate content. Manias et al. [3] used silicate nanomaterials and polymers to prepare a composite modified asphalt.

The test results showed that nanomaterials could make up for the shortcomings of a polymer-modified asphalt, and the stability, ablation resistance, and flame retardancy of composite modified asphalts were improved. Raufi et al. [4] studied the performance of a nano-$CaCO_3$ modified asphalt in a hot mix asphalt. The results showed that when the content of nano-$CaCO_3$ was 6%, the modified asphalt mixture had good moisture resistance and high temperature performance. Nejad et al. [5] modified an asphalt binder with SiO_2, TiO_2, and $CaCO_3$ nanoparticles, and studied the thermal properties of the modified binder. The results showed that the addition of these nanoparticles improved the glass transition temperature and low-temperature stiffness of the asphalt binder. Shafabakhsh et al. [6] found that for an asphalt binder modified with titanium dioxide nanoparticles, resistance to permanent deformation and the fatigue life of the asphalt mixture were improved. Azarhoosh et al. [7] added nano-TiO_2 to an asphalt binder to increase the adhesion of the asphalt to aggregates and extend the fatigue life of asphalt mixtures. Sun et al. [8,9] separately prepared a single modified asphalt and composite modified asphalt, and conducted comparative tests. The results showed that the composite modified asphalt and its mixture had better road performance. Ye et al. [10,11] tested the performance of nanometer titanium dioxide and SBS composite modified asphalt. The results showed that its high temperature stability was improved, the antirutting factor of asphalt concrete increased, but the change of fatigue factor was small.

At present, asphalt mixtures are generally modified with various fibers, including lignin fibers, polyester fibers, and glass fibers [12–15]. Basalt fiber (BF) is a new type of environmentally friendly mineral fiber made of basalt rock. It has the characteristics of high mechanical properties, low water absorption, and suitable temperature [16]. Wu et al. [17] studied the effects of basalt mineral fibers on the viscoelastic properties and high temperature stability of asphalt mixtures. The results showed that the incorporation of mineral fiber improved the dynamic modulus, rutting factor, dynamic stability, and flow value of the asphalt mixture in the high-temperature dynamic creep test, and improved the high-temperature performance as well. Cheng et al. [18] added BF to asphalt mortar and conducted softening point, cone penetration, viscosity, force extension, DSR (Dynamic Shear Rheometer), and BBR (Bending Beam Rheometer) tests. The results showed that the incorporation of BF improved the high-temperature and low-temperature performance of the asphalt mastic. Through analyzing the mixture's microstructure and morphology by scanning electron microscopy technique, Qin et al. [19] studied the effect of BF length and content on the performance of asphalt mortar. The microstructure and morphology of the mixture were analyzed by scanning electron microscopy. The results showed that the BF formed a three-dimensional network of dispersed stress in the asphalt mortar, which inhibited the crack development of the asphalt mortar, thereby improving the crack resistance. Wu et al. [20] analyzed the impact of basalt fibers on the toughness of AC-13 and SMA-13 asphalt mixtures. Through indirect tensile and scanning electron microscope tests, the effect of fiber on the toughness of the mixture and the toughening mechanism were analyzed. According to the research status of the low-temperature stability of BF, it could be found that the improvement mechanisms of BF on the asphalt mixture was that it formed a three-dimensional spatial grid structure, strengthened the toughness, and inhibited the propagation of cracks. Ren et al. [21] found that the fatigue failure of the asphalt mixture was mainly caused by the damage to the asphalt mortar, and that the addition of BF in asphalt mortar could effectively extend its fatigue life. Yang [22] studied the road performance and low-temperature characteristics of BF SMA-13 through low-temperature splitting, trabecular bending, and stress relaxation tests. The results showed that BF improved the low-temperature performance of the asphalt mixture. Wang et al. [23] studied the effects of BF on the asphalt binder and cement through fatigue tests. The BF released the stress concentration in the interface area of the two fillers, alleviated the fatigue damage caused by the cyclic load, and enhanced the antifatigue performance. Gu et al. [24] tested the performance of the BF asphalt mixture through DSR and repeated creep tests. The results showed that the BF-modified asphalt mastic had a high rutting factor and strong resistance to deformation at high temperatures. Gao [25] studied the performance of the BF-modified asphalt mixture through a low-temperature split test, and the toughness index showed that the

low-temperature crack resistance of BF-modified asphalt mixture was significantly improved. Based on the three-dimensional model and numerical analysis, Zhang et al. [26,27] studied the rheological and viscoelastic properties of basalt-fiber-reinforced asphalt mastic and mortar. The numerical analysis showed that the BF caused the stress redistribution of the asphalt mortar and reduced the stress of the asphalt mortar.

Compared with conventional regression model approach, the response ratio optimized by the response surface method is more accurate and is becoming increasingly popular in the construction industry [28]. The response surface method is a collection of statistical methods used for designing experiments, developing models, assessing the effects of the experimental factors, and optimizing the process [29,30]. Wang et al. [31] used the response surface methodology to study the effects of basalt fiber content, length, asphalt–aggregate ratio, and other factors on the volume and strength properties of SBS-modified asphalt mixture. Chavez et al. [32] applied the response surface method to evaluate the aging responses of asphalt binder. Moghaddam et al. [33] introduced the response surface method into the mix design for an asphalt mixture. According to the laboratory test results, it was finally determined that the optimal mix ratio was 5.88% whetstone and 0.18% PET (Polyethylene terephthalate) content. Based on the extensive literature, the response surface method can be successfully applied to study asphalt binders and mixtures.

In this study, an experimental scheme for a nano-TiO_2/$CaCO_3$ (NTC)-BF composite modified asphalt mixture was designed based on the response surface methodology. The NTC content, BF content, and asphalt–aggregate ratio were independent variables, while the density, Marshall stability, flow value, air voids, voids filled with asphalt (VFA), and voids in mineral aggregate (VMA) were responses or dependent variables. The relationships between preparation parameters and Marshall test indices were analyzed to evaluate the effects of the NTC content, BF content, and asphalt–aggregate ratio. A design optimization of the NTC-BF composite modified asphalt mixture was proposed and validated with experimental results.

2. Materials and Methods

2.1. Raw Materials

2.1.1. Asphalt

The matrix asphalt used in this paper was AH #90 from Panjin of Liaoning Province, China. The penetration, softening point, ductility, Brinell viscosity, and density of the asphalt were measured according to the "Testing Regulations for Asphalt and Asphalt Mixtures of Highway Engineering" (JTG E20-2011) [34]. The specific test results are listed in Table 1. In Table 1, the Brinell viscosity is the apparent viscosity of the asphalt measured with a Brookfield viscometer according to the specification JTG E20-2011 [34].

Table 1. Basic properties of neat asphalt.

Index	Result	Specification Limit
Penetration (25 °C, 5 s, 0.1 mm)	85.8	80–100
Softening Point $T_{R\&B}$ (°C)	46.9	≥45
Ductility (25 °C, cm)	>150	≥100
Brinell Viscosity (135 °C, Pa·s)	306.9	——
Density (15 °C, g/cm^3)	1.016	——

2.1.2. Basalt Fiber

The BF selected in the experiment comprised chopped fibers produced by Jilin Jiuxin Basalt Industry Co., Ltd. The test results of basalt fiber index parameters and the limits in the "Classification, Gradation, and Designation of Basalt Fiber" (GB/T 38111-2019) regulations [35] are shown in Table 2. The basic technical indicators are listed in Table 2. In addition to the basic technical indicators listed in

Table 2, the BF also has low hydrophilicity, high heat resistance, and high oil absorption (oil absorption rate of 6.154%), meaning the BF can be applied in composite modified asphalt.

Table 2. Technical index of basalt fiber (BF).

Index	Result	Specification Limit
Diameter (μm)	10–13	——
Length (mm)	6	——
Water Content (%)	0.030	≤0.2
Combustible Content (%)	0.56	——
Linear Density (Tex)	2398	2400 ± 120
Breaking Strength (N/Tex)	0.55	≥0.40
Tensile Strength (MPa)	2320	≥2000
Tensile Elastic Modulus (GPa)	86.3	≥85
Breaking Elongation (%)	2.84	≥2.5

Unit: 1Tex = 1g/km.

2.1.3. Nanomaterials

The selected NTC material (TC-816) was produced by Tiancheng High-Tech Nano-Composite Co., Ltd. It is a white material made of titanium dioxide (TiO_2) and inorganic synthetic materials via chemical methods. Its molecular formula is $TiO_2/CaCO_3$. The ratio of $TiO_2/CaCO_3$ is approximately 1:3.5. Its appearance is shown in Figure 1. The selected NTC material is chemically stable and hardly reacts with other elements or compounds at room temperature, and is insoluble in water. The support particles are rod-shaped, and the outer titanium dioxide particles are in the form of sheets (diameter 50–60 nm), which have a regular structure and excellent hiding power. According to the determination, the 45 micron sieve residue of the NTC material is 0.02% and the stacking density is 0.4 g/ml.

Figure 1. Appearance of nano-$TiO_2/CaCO_3$ (NTC).

2.1.4. Aggregates and Fillers

The coarse and fine aggregates selected in this paper were all from the Shuangyang quarry in Changchun City, Jilin Province, and the ore powder came from the limestone ore powder produced in Shuangyang Shixi, Changchun City, Jilin Province. The coarse and fine aggregates used in the test were screened step-by-step, which ensured the accuracy of the test and reduced the impact of the discreteness of the aggregates. According to the relevant requirements of the "Highway Engineering Aggregate Test Regulations" (JTG E42-2005) [36], the physical properties of coarse aggregates, fine aggregates, and mineral powder were tested. The results are shown in Tables 3–5.

Table 3. Basic technical aggregate index.

Sieve Size/mm	13.2	9.5	4.75	2.36	1.18	0.6	0.3	0.15	0.075
Apparent Relative Density γa	3.142	2.992	3.084	2.721	2.661	2.758	2.684	2.907	2.627
Relative Density of Surface Stem γs	3.066	2.943	3.001	2.646	2.602	2.709	2.635	2.820	2.528
Relative Density of Gross Volume γb	3.031	2.917	2.961	2.603	2.566	2.681	2.606	2.776	2.476
Water Absorption w_x (%)	1.17	0.86	1.35	1.67	1.38	1.07	1.13	2.14	2.04

Table 4. Basic technical index for the mineral powder.

Index	Unit	Measured Value	Specification Requirements (Highway Surface Layer)
Apparent Relative Density	g/cm^3	2.719	≥2.5
Water Content	%	0.19	≤1
Size Range < 0.6 mm	%	100	100
<0.15	%	95.1	90–100
<0.075	%	87.8	75–100
Outward Appearance		No agglomeration	No agglomeration
Hydrophilic Coefficient		0.68	<1

Table 5. Crushing and wear values of the coarse aggregate.

Technical Index	Measured Value	Specification Limit
Crush Value (%)	13.5	≤28
Wear Value (%)	16.0	≤30

2.2. Response Surface Methodology

The response surface methodology was originally used to optimize biological processes. When there are multiple influencing factors, the relationship between the influencing factors can be obtained by regression design method, so as to optimize the test process. Under the premise of considering random errors, this method selects fewer test points and reduces the amount of tests. After the test results are obtained, the results are fitted and a continuous variable regression surface model is established to finally obtain the optimal range of influence factors. Compared with the orthogonal test, the obtained response surface is a continuous surface model with greater visibility, and the model can be used to predict points outside the test range. This article only briefly introduces the response surface method. For details, see the literature [37].

The response surface methodology is constructed on the basis of the least-squares method. The optimization process is as follows. In the first step, assume the relationship between a corresponding value and multiple impact factors:

$$y = \mathrm{f}(x_1, x_2, \cdots, x_k) + \varepsilon, \tag{1}$$

In the formula, y is the response value; x_1, x_2, … … , x_k are the influence factors; ε is the random variable.

If there is an approximately linear relationship between the response value and the impact factor, then make a first-order Taylor expansion of Formula (1):

$$y = \beta_0 + \beta_1 x_1 + \beta_2 x_2 + \cdots + \beta_k x_k + \varepsilon, \tag{2}$$

In the Equation, β_i is the slope or linear effect of the influence factor x_i.

Fit the influence factor with the above Equation. If the fitting is successful, an appropriate influence factor can be selected to obtain the best response value. If it is found that the relationship between y

and xi cannot be expressed by the linear Taylor expansion, then the second-order transformation of Equation (2) needs to be further performed to obtain the following second-order model Equation:

$$y = \beta_0 + \sum_{i=1}^{k} \beta_i x_i + \sum_{i=1}^{k} \beta_{ii} x_i^2 + \sum_{i<j}^{k} \beta_{ij} x_i x_j + \varepsilon, \quad (3)$$

In the Equation, β_i is the linear effect of the independent variable x_i; β_{ij} is the interaction between the independent variables; B_{ii} is the secondary effect of x_i.

This can be expressed as a matrix:

$$Y = \beta_0 + X'b + X'BX + \varepsilon, \quad (4)$$

In the Equation, $X = (x_1, x_2, \cdots, x_k)^T$; $b = (\beta_1, \beta_2, \cdots, \beta_k)^T$ is the regression coefficient matrix; B is the k-th order symmetric matrix.

If the fitting is successful and the response reaches the best, then the following Equation is satisfied:

$$\frac{\partial Y}{\partial X} = \mathrm{b} + 2\mathrm{BX} = 0 \quad (5)$$

The solution X in Equation (5) is called the stable point, and the transformation can be obtained as:

$$X_0 = -\frac{1}{2} B^{-1} b, \quad (6)$$

Substituting Equation (6) into Equation (4), the predicted response value at the stable point is obtained as:

$$Y_0 = \beta_0 + \frac{1}{2} X_0' b, \quad (7)$$

There are many types of design models for response surface analysis, such as the central composite, Box–Behnken design, D-optimal design, and uniform design models. The specific design schemes of the various models are different, meaning the numbers of tests required are also different. It is necessary to select the appropriate model for the design according to the actual needs.

2.3. Test Design

The AC-13 gradation of asphalt mixtures is a fine-grained, continuous gradation, and is mostly used for pavement surface layer. Therefore, the asphalt mixture in this paper adopted the AC-13 gradation. The gradation of asphalt mixtures, including the upper limit, lower limit, median, and synthetic gradation curve values of the aggregates, are shown in Figure 2. The synthetic gradation was used in this study to mix the aggregates of multiple grades in proportion and close to the median value of the gradation. The gradation curve of the asphalt mixture is the same as in reference [38]. For the experimental design, this paper adopted the Box–Behnken method. NTC and BF are asphalt admixtures. The upper and lower limits of admixtures and the ranges of asphalt ratios were determined according to the literature [10,39–41]. The selected three impact factor levels are shown in Table 6.

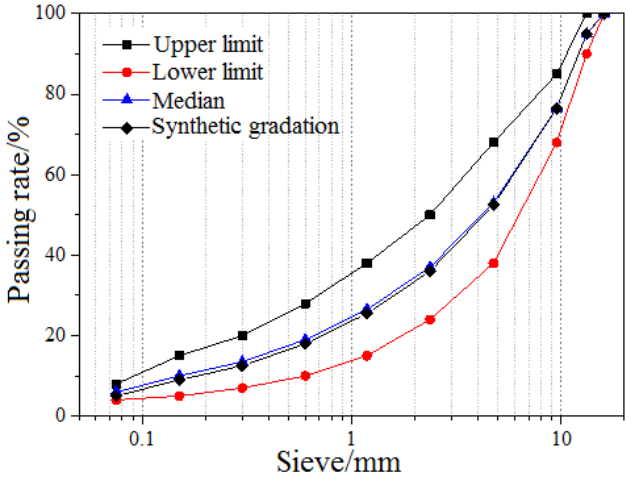

Figure 2. AC-13 gradation curve of the asphalt mixture.

Table 6. Influence factor level and design.

Impact Factor	Name	Unit	Minimum	Maximum	Level		
					−1	0	1
A	Fiber Content	%	1.00	7.00	1.0	4.0	7.0
B	NTC Content	%	1.00	9.00	1.0	5.0	9.0
C	Asphalt–aggregate ratio	%	4.00	7.00	4.0	5.5	7.0

In this study, the asphalt–aggregate ratio is measured by weight.

The Box–Behnken test design has an impact factor range of 3–7, which can better evaluate the non-linear correlation between the response index and the impact factor. Under the same conditions, the number of tests required is less than other methods. In the Box–Behnken test design, the number of tests required for the three impact factors was 17. There were six response output indicators that needed to be determined in the experiment, namely the density, Marshall stability, flow value, air voids, VMA, and VFA of the asphalt mixture. The impact factors of the 17 groups of experiments are set out in Table 7 below.

Table 7. Optimization of test design.

Numbering	BF Content (%)	NTC Content (%)	Asphalt–Aggregate Ratio (%)
1	1.0	5.0	4.0
2	1.0	5.0	7.0
3	4.0	5.0	5.5
4	7.0	5.0	7.0
5	4.0	5.0	5.5
6	4.0	1.0	7.0
7	1.0	9.0	5.5
8	4.0	9.0	4.0
9	4.0	1.0	4.0
10	7.0	5.0	4.0
11	1.0	1.0	5.5
12	7.0	1.0	5.5
13	4.0	5.0	5.5
14	4.0	5.0	5.5
15	4.0	5.0	5.5
16	7.0	9.0	5.5
17	4.0	9.0	7.0

2.4. Response Output Index Test Method

2.4.1. Production of Asphalt Mixture Test Piece

The asphalt mixtures were prepared according to JTG E20-2011 [34]. When preparing modified asphalt, the control asphalt and NTC were mixed using blending equipment at a speed of 4000 r/min for 45 min. The temperature for the mixing process was 150 °C. When preparing the asphalt mixture, the aggregates and the BF were mixed at a temperature of 160 °C. Then, the modified asphalt was poured in and mixed until the aggregates were coated. Next, the weighted fillers were added and mixed well. The Marshall specimens in this study were prepared at a height of 63.5 ± 1.3 mm and diameter of 101.6 ± 0.2 mm. The double-sided compaction occurred 75 times.

2.4.2. Measurement and Calculation of the Volume Index

According to the requirements of JTG E20-2011 [34], the dry surface method was used to determine the relative gross weight density, gross bulk density, air voids, mineral air voids, and VFA of the asphalt mixture. The specific calculation Equation was as follows:

$$\gamma_f = \frac{m_a}{m_f - m_w}, \tag{8}$$

$$\rho_f = \frac{m_a}{m_f - m_w} \times \rho_w, \tag{9}$$

In the Equation, γ_f is the relative density of the wool volume of the specimen, which is dimensionless; m_a is the air weight of the dried specimen; m_f is the surface dry weight of the specimen; m_w is the weight of the test piece in water (g); ρ_f is the test piece of the gross volume density; ρ_w is the density of the water at 25 °C, the value of which is 0.9971 g/cm^3.

$$\mathrm{VV} = \left(1 - \frac{\gamma_f}{\gamma_t}\right) \times 100, \tag{10}$$

In the Equation, γ_f is the maximum theoretical density of the asphalt mixture, which is dimensionless; γ_t is the relative density of the asphalt mixture gross volume, which is dimensionless.

$$\mathrm{VMA} = \left(1 - \frac{\gamma_f}{\gamma_{sb}} \times \frac{p_s}{100}\right) \times 100, \tag{11}$$

In the Equation, VMA is the aggregate gap ratio of asphalt mixture; γ_{sb} is the relative density of the synthetic wool volume of the mixture, which is dimensionless; p_s is the sum of the percentage of various mineral materials in the total mass of the asphalt mixture.

$$\mathrm{VFA} = \frac{VMA - VV}{VMA} \times 100\%, \tag{12}$$

In the Equation, VFA represents the voids filled with asphalt in the mixture.

2.4.3. Determination of Marshall Stability Test Index

According to the requirements of JTG E20-2011 [34], after the test specimen was kept in a constant temperature water bath at 60 ± 1 °C for 30–40 minutes, the Marshall tester was used to test the Marshall stability and flow value of the test piece.

3. Results and Discussion

The test results are shown in Table 8. After obtaining the statistics for the test data, the maximum value, minimum value, average value, and standard deviation of each output index could be obtained, which could be used as the basis for further analysis. The results are shown in Table 9.

Table 8. Marshall test results. VMA, voids in mineral aggregate; VFA, voids filled with asphalt.

Test Serial Number	A	B	C	Density (g/cm^3)	Air Voids (%)	Marshall Stability (kN)	Flow Value (mm)	VMA (%)	VFA (%)
1	1.0	5.0	4.0	2.383	6.9	10.30	1.9	13.0	46.5
2	1.0	5.0	7.0	2.365	3.9	8.57	3.6	16.1	75.6
3	4.0	5.0	5.5	2.423	3.4	13.37	2.5	12.8	73.2
4	7.0	5.0	7.0	2.358	4.2	9.73	2.7	16.3	74.3
5	4.0	5.0	5.5	2.423	3.4	13.37	2.5	12.8	73.2
6	4.0	1.0	7.0	2.349	5.9	9.92	3.7	16.6	64.2
7	1.0	9.0	5.5	2.408	1.3	12.10	2.9	12.2	89.2
8	4.0	9.0	4.0	2.356	8.2	10.53	1.8	14.0	41.2
9	4.0	1.0	4.0	2.330	8.7	9.83	2.3	14.9	41.8
10	7.0	5.0	4.0	2.324	9.2	10.79	2.1	15.1	38.9
11	1.0	1.0	5.5	2.355	5.6	11.52	2.8	15.2	62.7
12	7.0	1.0	5.5	2.344	6.1	11.65	2.6	15.6	60.7
13	4.0	5.0	5.5	2.423	3.4	13.37	2.5	12.8	73.2
14	4.0	5.0	5.5	2.430	3.4	13.37	2.5	12.8	73.2
15	4.0	5.0	5.5	2.430	3.4	13.37	2.5	12.8	73.2
16	7.0	9.0	5.5	2.392	4.1	11.15	3.3	13.2	68.4
17	4.0	9.0	7.0	2.381	3.6	10.06	2.4	15.5	76.6

For the convenience of calculation, test groups with the same impact factor level are calculated using the same test data.

Table 9. Total test results.

Project	Name	Unit	Min.	Max.	Average	Standard Deviation
Y1	Density	g/cm^3	2.324	2.431	2.380	0.0355
Y2	Air Voids	%	1.3	9.3	5.0	2.2226
Y3	Marshall Stability	kN	8.57	13.38	11.36	1.5741
Y4	Flow Value	mm	1.8	3.7	2.7	0.5265
Y5	VMA	%	12.3	16.7	14.3	1.5146
Y6	VFA	%	38.9	89.2	65.1	14.6017

3.1. Analysis of Response Output Index Results

3.1.1. Density

By analyzing the linear model (linear), two-factor model (2FI), and quadratic equation model (quadratic), the best fitting equation model was found and the coefficient of determination R^2 was used to evaluate the fit.

The impact factor was fitted to the three model equations, and SST (sum of squares total) of each model was calculated. Then, the SST was decomposed:

$$\mathrm{SST} = \Sigma(Y_i - \overline{Y})^2 = \Sigma(Y_i - \overline{Y}_i)^2 + 2\Sigma\left(Y_i - \hat{Y}_i\right)\left(\hat{Y}_i - \overline{Y}\right) + \Sigma(\hat{Y}_i - \overline{Y})^2, \quad (13)$$

$$\Sigma\left(Y_i - \hat{Y}_i\right)\left(\hat{Y}_i - \overline{Y}\right) = \Sigma e_i\left(\hat{Y}_i - \overline{Y}\right) = 0, \quad (14)$$

Therefore, the total dispersion was finally decomposed into the following Equation:

$$\mathrm{SST} = \Sigma(Y_i - \overline{Y})^2 = \Sigma(Y_i - \overline{Y}_i)^2 + \Sigma(\hat{Y}_i - \overline{Y})^2 = SSR + SSE, \quad (15)$$

In the Equation, SSR is the sum of squares within the group (regression square sum); SSE is the sum of squares between groups (sum of squared residuals).

The solvability coefficient R^2 is as follows:

$$R^2 = \frac{SSR}{SST} = 1 - \frac{SSE}{SST}, \tag{16}$$

The closer SSR is to SST, the smaller the residual is and the closer R^2 is to 1, indicating a higher degree of fit. In order to exclude the influence of too many variables on the degree of fit, R^2 was adjusted by the following Equation to obtain the predicted $\overline{R}^2$:

$$\overline{R}^2 = 1 - \frac{SSE/(n-k-1)}{SST/(n-1)}, \tag{17}$$

In the Equation, $n-k-1$ is the degree of freedom of the sum of squares between groups; $n-1$ is the degree of freedom of the sum of squares of the total dispersion.

Table 10 lists the comparison results after fitting with various equations.

Table 10. Comprehensive analysis of fitting degree. 2FI, two-factor model.

Types	Continuous P Value	Out-of-Fit P Value	Correct R^2	Predict R^2	Result
Linear	0.3169	<0.0001	0.0528	−0.1622	—
2FI	0.9247	<0.0001	−0.1768	−0.9142	—
Quadratic	<0.0001	<0.0001	0.9416	0.5912	Recommended

After analyzing the fitting degree of each model, it was found that the highest fitting degree was the quadratic equation model. The F test was carried out to assess the variance and misfit values of each regression model. Here, we take the linear model as an example.

For the test model:

$$Y_I = \beta_0 + \beta_1 X_{1i} + \beta_2 X_{2i} + \cdots + \beta_k X_{ki} + u_i,\ i = 1, 2, \cdots, n \tag{18}$$

If the parameter is significantly non-zero, the following null hypothesis and alternative hypothesis are made:

$H_0 : \beta_1 = \beta_2 = \cdots = \beta_k = 0$ $H_1 : \beta_i$ is not all 0.

$$\mathrm{F} = \frac{\overline{R}^2/k}{\left(1-\overline{R}^2\right)(n-k-1)} \tag{19}$$

It can be found that when R^2 approaches 0, the F value also approaches 0; when R^2 approaches 1, the F value approaches infinity. Therefore, the test hypothesis H_0 is equivalent to the test $R^2 = 0$. Tables 11–13 list the results for the analysis of variance for each fitted model.

According to the analysis of the above tables, it is found that the quadratic equation had the highest degree of fitting, which was recommended. The variance of each variable fitted by the quadratic equation is analyzed below, and the results are shown in Table 14.

Table 11. Variance analysis of multiple models.

Source of Variance	Sum of Squares	Degrees of Freedom	Mean Square	F Value	Probability > F	Result
Mean vs. Total	96.3291	1	96.3291	—	—	—
Linear vs. Mean	0.0046	3	0.0015	1.2978	0.3169	—
2FI vs. Linear	0.0006	3	0.0002	0.1540	0.9247	—
Quadratic vs. 2FI	0.0143	3	0.0047	64.8540	<0.0001	Recommended
Residual	2.59×10^{-12}	4	6.48×10^{-13}	—	—	—
Total	96.349	17	5.6676	—	—	—

Table 12. Unverified verification.

Source of Variance	Sum of Squares	Degrees of Freedom	Mean Square	F Value	Probability > F	Result
Linear	0.0155	9	0.0017	2.65×10^{-9}	<0.0001	—
2FI	0.0148	6	0.0024	3.81×10^{-9}	<0.0001	—
Quadratic	0.0005	3	0.0001	2.64×10^{-8}	<0.0001	Recommended
Pure error	2.59×10^{-12}	4	6.48×10^{-13}	—	—	—

Table 13. Model summary statistics.

Types	Sample Standard Deviation	Fit	Corrected Fit	Prediction Fit	Result
Linear	0.0345	0.2304	0.0528	-0.1622	—
2FI	0.0385	0.2644	−0.1768	−0.9142	—
Quadratic	0.0085	0.9744	0.9416	0.5912	Recommended
Cubic	8.0538×10^{-7}	1	0.9999	—	Poor

Table 14. Density variance test.

Project	Sum of Squares	Degrees of Freedom	Mean Square Error	F Value	P Value	Significant
Model	0.02	9	2.18×10^{-3}	29.67	<0.0001	√
A: Fiber Content	1.08×10^{-3}	1	1.08×10^{-3}	14.6	0.0065	√
B: Nano-Material Content	3.13×10^{-3}	1	3.13×10^{-3}	42.5	0.0003	√
C: Asphalt–Aggregate Ratio	4.46×10^{-4}	1	4.46×10^{-4}	6.06	0.0434	√
AB	3.96×10^{-6}	1	3.96×10^{-6}	0.054	0.8233	×
AC	6.72×10^{-4}	1	6.72×10^{-4}	9.14	0.0193	√
BC	9.27×10^{-6}	1	9.27×10^{-6}	0.13	0.7331	×
A^2	2.11×10^{-3}	1	2.11×10^{-3}	28.64	0.0011	√
B^2	2.86×10^{-3}	1	2.86×10^{-3}	38.88	0.0004	√
C^2	8.01×10^{-3}	1	8.01×10^{-3}	108.77	<0.0001	√
Residual	5.15×10^{-4}	7	7.36×10^{-5}	—	—	—
Mismatch	5.15×10^{-4}	3	1.72×10^{-4}	—	—	—
Pure Error	0	4	0	—	—	—
Total Deviation	0.02	16	—	—	—	—

According to the results of analysis of variance, the fitting equation of the response index can be obtained:

$$\text{Density} = 1.78911 + 5.94747 \times 10^{-4} \times A + 0.020 \times B + 0.205 \times C - 8.289 \times 10^{-5} \times A \times B + 0.0029 \times A \times C + 2.53744 \times 10^{-4} \times B \times C - 0.0024862 \times A^2 - 1.62926 \times 10^{-3} \times B^2 - 0.019378 \times C^2$$

In the Equation, A is the amount of BF; B is the amount of NTC; C is the asphalt–aggregate ratio.

The distribution of predicted and measured values is shown in Figure 3.

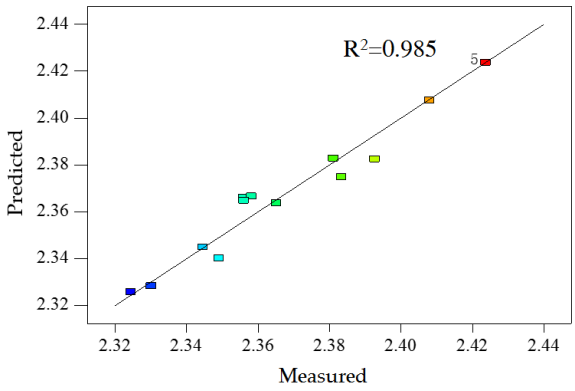

Figure 3. The measured and predicted values for density.

Figure 3 shows the relationship between the response index predicted by the final equation and the measured values. The smaller the distance between the point and the diagonal, the higher the accuracy of the prediction; the greater the degree of deviation from the top to the bottom, the greater the error. It can be seen that there are seven sets of measured values that coincide with the predicted values, and there are six sets of measured values that are distributed on the diagonal line but not far away. There are no outliers in the whole distribution, which indicates that the method of obtaining the predicted value via the fitting equation is reliable.

Three-dimensional coordinates can only represent the effects of two impact factors at the same time, so when analyzing the interaction of the two factors, the third impact factor is taken as the median value within the range and is fixed. The contour plot and response surface plot between the density and each influencing factor are shown in Figure 4.

It can be seen from Figure 4 that the location with the highest density is in the middle dark parts of the contour plot and the response surface plot. There are five measured points in each surface graph, indicating how well the predicted surface fits the actual values. It can be found from the surface graph that the predicted values fit the surface better. Increasing the amount of NTC and BF makes the mixture density increase first and then decrease, however the two factors influence each other. Under the premise that the asphalt–aggregate ratio is 5.5%, the effect of the fiber content on density gradually increases during the increase of the NTC content from 1% to 7%. In the process of increasing the fiber content from 3.5% to 9%, the effect of NTC on the density decreases slightly. In addition, as the asphalt–aggregate ratio increases, the density of the mixture increases first and then decreases.

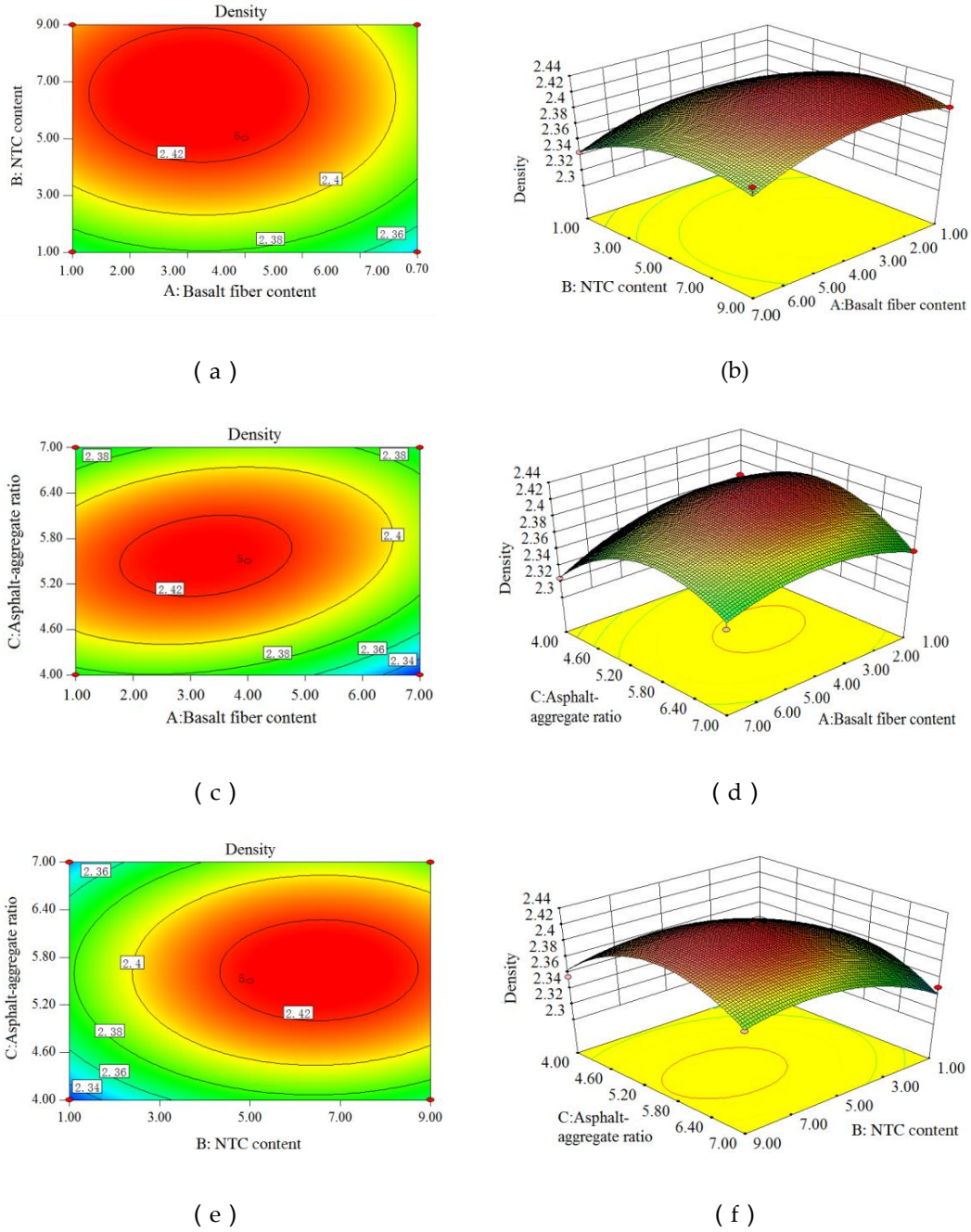

Figure 4. Contour map and response surface map of density and influencing factors. (**a**) Contour map between basalt fiber content, NTC content and density; (**b**) Three-dimensional surface graph between basalt fiber content, NTC content and density: (**c**) Contour map between basalt fiber content, asphalt–aggregate ratio and density; (**d**) Three-dimensional surface graph between basalt fiber content, asphalt–aggregate ratio and density; (**e**) Contour map between asphalt–aggregate ratio, NTC content and density; (**f**) Three-dimensional surface graph between asphalt–aggregate ratio, NTC content and density.

3.1.2. Air Voids

The comparison of the fitting degrees of various fitting equations in the air voids analysis is consistent with the method selected in the density analysis process in the previous section, and will not be repeated in this section. Table 15 is the variance test situation of each variable after fitting through the quadratic equation.

Table 15. Air voids variance test table.

Project	Sum of Squares	Degrees of Freedom	Mean Square Error	F Value	P Value	Significant
Model	77.35	9	8.59	35.59	<0.0001	√
A: Fiber Content	4.32	1	4.32	17.9	0.0039	√
B: Nano-Material Content	10.46	1	10.46	43.31	0.0003	√
C: Asphalt–Aggregate Ratio	29.83	1	29.83	123.52	<0.0001	√
AB	1.42	1	1.42	5.87	0.0459	√
AC	1.01	1	1.01	4.2	0.0797	×
BC	0.86	1	0.86	3.56	0.1013	×
A^2	0.13	1	0.13	0.53	0.4909	×
B^2	2.2	1	2.2	9.11	0.0194	√
C^2	25.86	1	25.86	107.08	<0.0001	√
Residual	1.69	7	0.24	—	—	—
Mismatch	1.69	3	0.56	—	—	—
Pure Error	0	4	0	—	—	—
Total Deviation	79.04	16	—	—	—	—

According to the analysis of variance results, the fitting equation for the air voids can be obtained:

Air voids = 42.12238 + 0.45739 × A − 0.51128 × B − 12.56855 × C + 0.049613 × A × B − 0.111 × A × C − 0.077228 × B × C + 0.0193422 × A^2 + 0.045175 × B^2 + 1.10135 × C^2

The distribution of the predicted and measured values is shown in Figure 5.

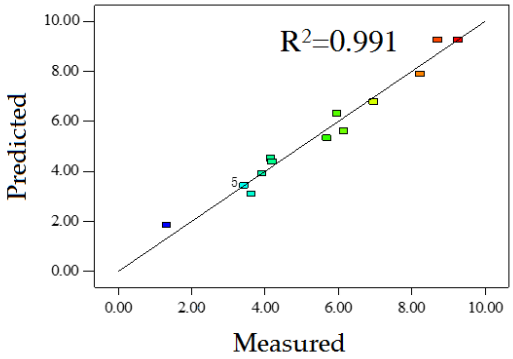

Figure 5. The measured and predicted values of the air voids.

It can be seen from the above figure that the fit between the predicted value and the measured value is good, indicating that the fitting equation was selected accurately. There are 5 test groups with air void contents greater than 6% in the figure, exceeding the "Technical Specifications for Highway Asphalt Pavement Construction" (JTG F40-2004) regulations [42]; therefore, it is necessary to limit the scope when optimizing the impact factor.

Using the same method as Section 3.1.1, the contour plot and the response surface plot between the air voids and each influencing factor were drawn. The results are shown in Figure 6.

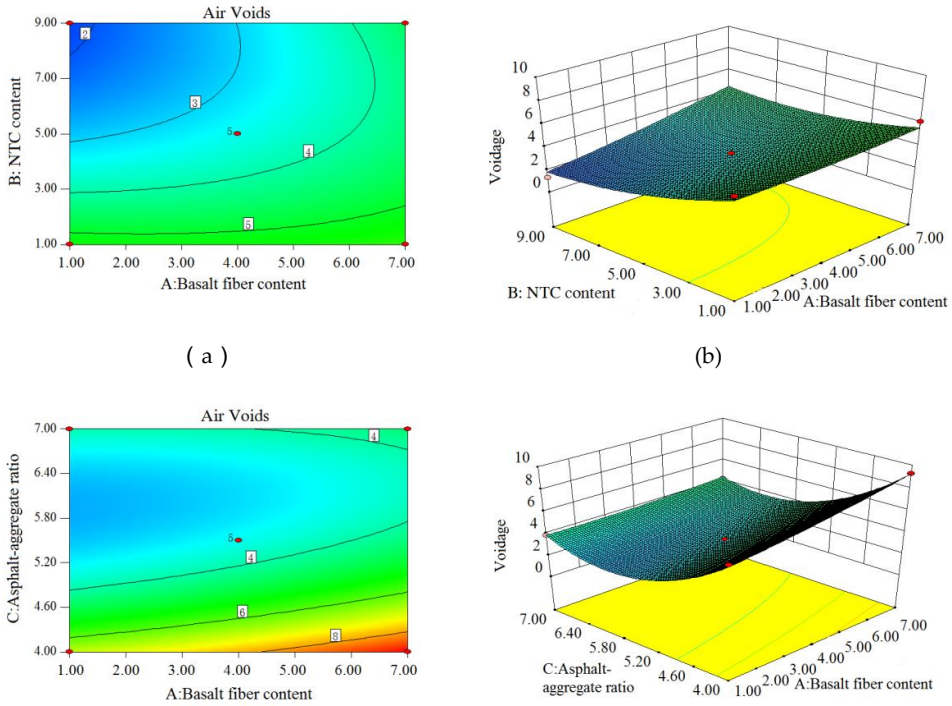

Figure 6. *Cont.*

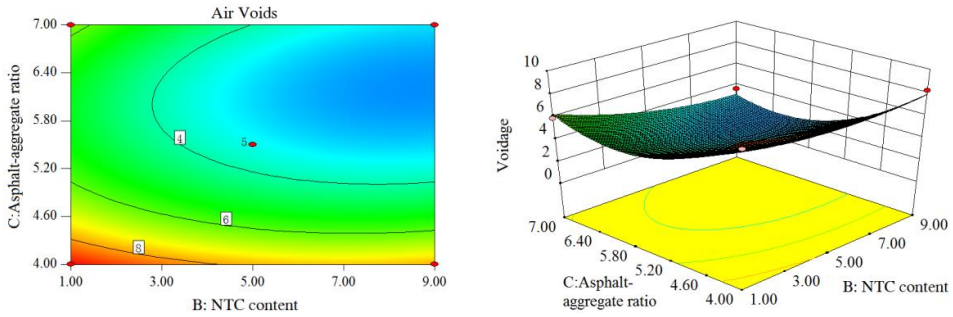

(e) (f)

Figure 6. Contour maps and response surface maps of the air voids and influencing factors. (**a**) Contour map between basalt fiber content, NTC content and air voids; (**b**) Three-dimensional surface graph between basalt fiber content, NTC content and air voids: (**c**) Contour map between basalt fiber content, asphalt–aggregate ratio and air voids; (**d**) Three-dimensional surface graph between basalt fiber content, asphalt–aggregate ratio and air voids; (**e**) Contour map between asphalt–aggregate ratio, NTC content and air voids; (**f**) Three-dimensional surface graph between asphalt–aggregate ratio, NTC content and air voids.

According to Figure 6, the addition of BF leads to an increase of the air voids in the asphalt mixture, while the addition of NTC reduces the air voids in the asphalt mixture; the interaction between NTC and the BF modifier is obvious. On the premise that the asphalt–aggregate ratio is 5.5%, when the NTC content is 1.0% the fiber content increases from 1.0% to 7.0%, while the air voids only increase by about 1.0%. When the NTC content is 9.0%, the fiber content increases from 1.0% to 7.0% and the air voids increase by about 3.0%. When the fiber content is 1.0%, during the increase of the NTC content the air voids decreases by about 4.0% and the effect is more obvious. When the fiber content is 7.0%, the increase of NTC reduces the air voids by about 1.0% and the effect is greatly reduced. The increase of the asphalt–aggregate ratio makes the air voids of the mixture decrease first and then increase. When the asphalt–aggregate ratio is relatively high or low the influences of fiber and NTC are reduced, and when the asphalt–aggregate ratio is moderate the effects of the two are amplified.

3.1.3. Marshall Stability

The quadratic equation was selected as the design model for the fitting calculation. Then, the variance test was performed. The results are shown in Table 16.

Table 16. Marshall stability variance test table.

Project	Sum of Squares	Degrees of Freedom	Mean Square Error	F Value	P Value	Significant
Model	38.08	9	4.23	18.95	0.0004	√
A: Fiber Content	0.086	1	0.086	0.39	0.5543	×
B: Nano-Material Content	0.11	1	0.11	0.48	0.5112	×
C: Asphalt–aggregate Ratio	1.25	1	1.25	5.61	0.0497	√
AB	0.29	1	0.29	1.29	0.2928	×
AC	0.11	1	0.11	0.51	0.4982	×
BC	0.076	1	0.076	0.34	0.5788	×
A^2	4.24	1	4.24	19	0.0033	√
B^2	2.46	1	2.46	11.04	0.0127	√
C^2	26.79	1	26.79	119.98	<0.0001	√
Residual	1.56	7	0.22	—	—	—
Mismatch	1.56	3	0.52	—	—	—
Pure Error	0	4	0	—	—	—
Total Deviation	39.64	16	—	—	—	—

According to the analysis of variance, the fitting equation of the Marshall stability can be obtained:

Marshall stability = $-22.60123 + 0.832535 \times A + 0.72266 \times B + 12.03306 \times C - 0.022396 \times A \times B + 0.037500 \times A \times C - 0.022917 \times B \times C - 0.1115278 \times A^2 - 0.047813 \times B^2 - 1.12111 \times C^2$

The distribution of the predicted and measured values is shown in Figure 7.

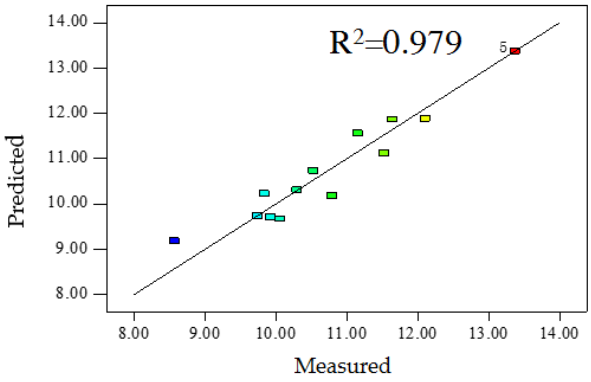

Figure 7. The measured value and the predicted value for the Marshall stability.

It can be seen from the above figure that the fit between the predicted value and the measured value obtained by the equation is good, indicating that the fitting equation was selected accurately. Using the same method as Section 3.1.1, the contour plots and the response surface plots between the Marshall stability and each influence factor were drawn. The results are shown in Figure 8.

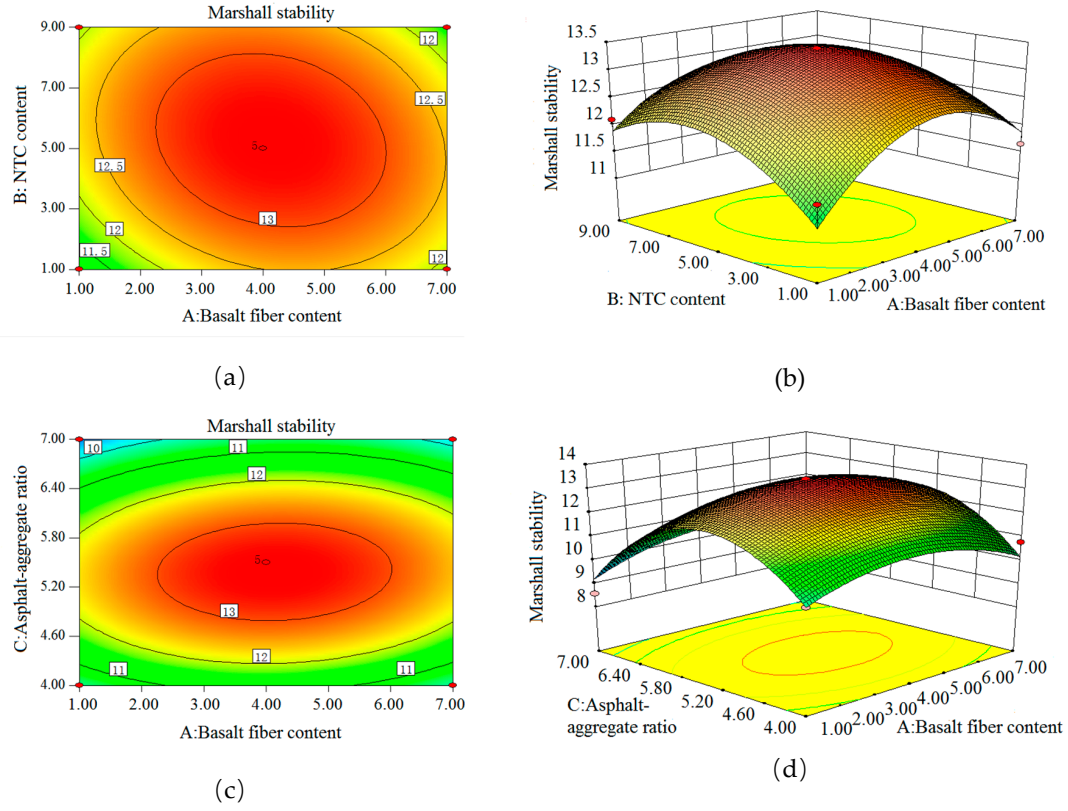

Figure 8. *Cont.*

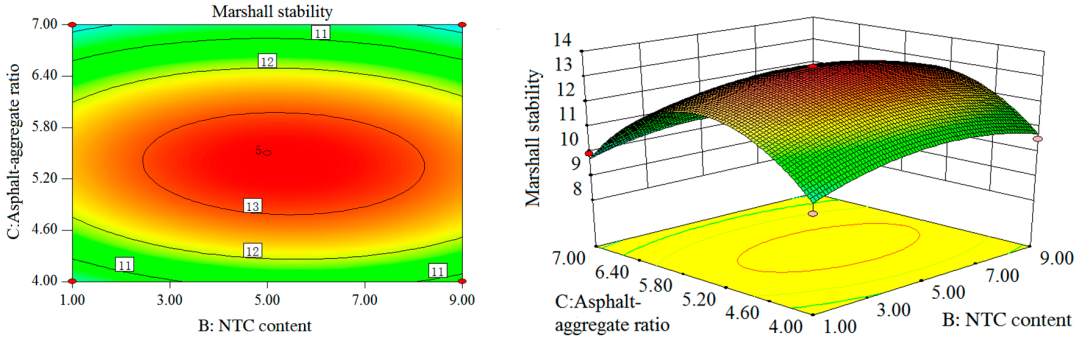

(e) (f)

Figure 8. Contour maps and response surface maps of the Marshall stability and influencing factors. (**a**) Contour map between basalt fiber content, NTC content and Marshall stability; (**b**) Three-dimensional surface graph between basalt fiber content, NTC content and Marshall stability: (**c**) Contour map between basalt fiber content, asphalt–aggregate ratio and Marshall stability; (**d**) Three-dimensional surface graph between basalt fiber content, asphalt–aggregate ratio and Marshall stability; (**e**) Contour map between asphalt–aggregate ratio, NTC content and Marshall stability; (**f**) Three-dimensional surface graph between asphalt–aggregate ratio, NTC content and Marshall stability.

It can be seen from the surface graph that the incorporation of fiber and NTC significantly improves the Marshall stability of the asphalt mixture, but as the amount of both increases the Marshall stability first increases and then decreases. When the content of the fiber or NTC is too high or too low, the influence of other modifiers on the Marshall stability will become greater. The asphalt–aggregate ratio has a greater influence on the Marshall stability. The Marshall stability of the mixture will increase first and then decrease with the increase of the asphalt–aggregate ratio.

3.1.4. Three Other Response Indicators

The three response indicators are analyzed above. The analysis process of the other three response indicators is similar, and their respective fitting equations are given here.

The fitting equation of the flow value is:

$$\text{Flow value} = 0.90820 - 0.021562 \times A - 0.029375 \times B + 0.36354 \times C$$

The fitting equation of the VMA is:

$$\text{VMA} = 33.66448 + 0.169484 \times A - 0.67940 \times B - 7.61505 \times C + 0.010606 \times A \times B - 1.05540 \times A \times C - 7.89220 \times 10^{-3} \times B \times C + 0.0641631 \times A^2 + 0.044624 \times B^2 + 0.79113 \times C^2$$

The fitting equation of the VMA is:

$$\text{VFA} = -167.08156 - 1.246516 \times A + 1.85955 \times B + 76.06018 \times C - 0.391630 \times A \times B + 0.345055 \times A \times C + 0.53780 \times B \times C - 0.0014281 \times A^2 - 0.18114 \times B^2 - 6.35841 \times C^2$$

3.2. Input Index Optimization Based on Response Surface Fitting Model

It can be seen from the analysis of the variance of each response index that the influence of each input index on the response value can be fitted by the equation. It is difficult to obtain the optimal solutions of the three impact factors through the Marshall test. Therefore, it was necessary to set the range and expected value of each response index in the program. Then, the continuous surface model was fitted and a series of input index combinations were predicted.

The response output index range was selected with reference to the relevant index range in the Marshall test and the selection of each expected value was adjusted according to the situation. According to the regulations in JTG F40−2004 [42], the response output index range was selected. There is no requirement for the density range in JTG F40−2004 [42] and the range target value was set as the maximum density. The required range of air voids was 3.0–5.5%, and the target value was set at a median value of 4%. The target value of Marshall stability was set as the maximum value. The specified

range of flow value was 2.0 mm–4.0 mm and the target value was set as the median value of 3.0 mm. The provisions of VMA were not less than 14%. The requirements of VFA were 65–75%. The expected value of the mixture with the highest Marshall stability and the best Marshall stability is the desired result. The predicted values after optimization under the optimal conditions are shown in Table 17.

Table 17. Model optimization factor and prediction index values.

Fiber Content (%)	NTC Content (%)	Asphalt–Aggregate Ratio (%)	Density (g/cm^3)	Air Voids (%)	Marshall Stability (kN)	Flow Value (mm)	VMA (%)	VFA (%)
3.9	5.1	5.67	2.4237	3.4	13.29	2.7	14.9	73.2

3.3. Model Validation

In order to verify the accuracy of the prediction results of the response surface methodology, the optimum asphalt–aggregate ratio (5.67%) and the mixture ratio of BF (3.9%) and NTC (5.1%) were selected as the formed specimens. The sample preparation process was the same as Section 2.4.1. The Marshall results were compared and verified. There were 6 test pieces in each group in the verification tests. The results are shown in Table 18.

Table 18. Accuracy rate of the response surface methodology.

Project	Density (g/cm^3)	Air Voids (%)	Marshall Stability (kN)	Flow Value (mm)	VMA (%)	VFA (%)
1	2.431	3.436	17.22	1.8	16.7	56.9
2	2.399	4.516	12.59	2.3	14.6	84.2
3	2.497	4.593	16.13	2.9	13.9	80.1
4	2.428	5.22	15.62	1.9	12.3	71.6
5	2.429	1.384	11.75	3.8	15.6	77.3
6	2.396	1.413	11.71	4.7	13.9	67.3
Average Value	2.430	3.427	14.17	2.9	14.5	72.9
Standard Deviation	0.033	1.527	2.223	1.050	1.392	9.018
Prediction Data	2.424	3.43	13.29	2.7	14.9	73.2
Error (%)	0.270	0.096	6.620	6.960	2.759	0.370

According to the data obtained from the verification test and the prediction data of the response surface method, the errors of the predicted response value and the experimental value are shown in Table 18. The maximum error was 6.960% and the minimum error was 0.096%. This shows that in the research on the mix ratio of the asphalt concrete, it was feasible to use the response surface method to optimize the selection of the best impact factor.

4. Conclusions

Based on the response surface method, this research adopted the Box–Behnken design method to carry out a three−factor, three−level design. Density, air voids, Marshall stability, flow value, VMA, and VFA values were used as response indicators, while the asphalt–aggregate ratio, NTC, and fiber contents were taken as influencing factors. This method is more logical and predictable when determining the optimal content of various factors. This paper draws the following conclusions through experimental analysis:

(1) Through the Box–Behnken design method, a three−factor function was fitted to each response indicator. It is concluded that the relationship between density, air voids, Marshall stability, VMA, VFA, and the three influencing factors is a quadratic function, and the relationship between the flow value and the three influencing factors is linear;

(2) Through analysis of variance and testing of the fitted model, it is concluded that the fitted model has a higher significance level. Comparing the predicted value with the measured value, it is found that the difference between them is small. This shows that the model has high fitting

accuracy and prediction ability, and can accurately reflect the relationship between each input index and output index;

(3) Through comprehensive consideration of the response index values, the three influencing factors are optimized and predicted, and the optimal content of NTC, BF, and the optimal asphalt–aggregate ratio are 5.1%, 3.9%, and 5.67%, respectively. The response index value is obtained through model test prediction, while the measured data is compared with the predicted value to obtain a minimum relative error of 0.096% and a maximum error of 6.960%. This shows that the response surface method can be used to design, analyze, optimize, and predict the mix ratio of the asphalt mixture.

Author Contributions: Conceptualization, H.B.; formal analysis, Y.G., H.B., and J.S.; investigation, Y.G.; data curation, H.B. and J.S.; writing—original draft preparation, J.S. and Z.T.; writing—review and editing, Y.G. and Z.T.; project administration, Y.G. and J.S.; funding acquisition, Y.G. and Z.T. All authors have read and agreed to the published version of the manuscript.

Funding: This work was supported by the Transportation Technology Program of Jilin Province of China (Grant No. 2018ZDGC−16, 2018−1−9), the Education Department's "13th Five−Year" Science and Technology Program of Jilin Province (Grant No. JJKH20190015KJ), the Fundamental Research Funds for the Central Universities and the Scientific and Technological Developing Scheme Program of Jilin Province (Grant No. 20200403157SF).

Acknowledgments: We would like to acknowledge the following people from Jilin University. Thank you to Wensheng Wang, Bo Wang, Yulin Ma, and Yang He for technical support in the testing procedure and data processing.

Conflicts of Interest: The authors declare that there is no conflict of interest regarding the publication of this paper.

References

1. Huang, B.; Ma, L.P.; Xu, W.J. Research Development of Modified Asphalt. *Mater. Her.* **2010**, *24*, 137–141.
2. Chang, H.Z.; Zhang, H.L. Research on Performance and Mechanism of Nano−$CaCO_3$/SBS Composite Modified Asphalt. *Highw. Transp. Technol. Appl. Technol. Ed.* **2013**, *9*, 28–31.
3. Manias, E.; Touny, A.; Wu, L.; Lu, B.; Strawhecker, K.; Gilman, J.W.; Chung, T.C. Polypropylene/Silicate Nanocomposites, Synthetic Routes and Materials Properties. *Chem. Mater.* **2001**, *13*, 3516–3523. [CrossRef]
4. Raufi, H.; Topal, A.; Kaya, D.; Sengoz, B. Performance Evaluation of Nano−$CaCO_3$ Modified Bitumen in Hot Mix Asphalt. In Proceedings of the 18th IRF World Road Meeting, Delhi, India, 14–17 November 2017.
5. Nejad, F.M.; Nazari, H.; Naderi, K.; Karimiyan Khosroshahi, F.; Hatefi Oskuei, M. Thermal and rheological properties of nanoparticle modified asphalt binder at low and intermediate temperature range. *Pet. Sci. Technol.* **2017**, *35*, 641–646. [CrossRef]
6. Shafabakhsh, G.; Mirabdolazimi, S.M.; Sadeghnejad, M. Evaluation the effect of nano−TiO_2 on the rutting and fatigue behavior of asphalt mixtures. *Constr. Build. Mater.* **2014**, *54*, 566–571. [CrossRef]
7. Azarhoosh, A.R.; Nejad, F.M.; Khodaii, A. Using the Surface Free Energy Method to Evaluate the Effects of Nanomaterial on the Fatigue Life of Hot Mix Asphalt. *J. Mater. Civ. Eng.* **2016**, *28*, 04016098.1–04016098.9. [CrossRef]
8. Sun, L.; Xin, X.T.; Wang, H.Y.; Gu, W.J. Performance of nanomaterials modified asphalt binders. *J. Chin. Ceram. Soc.* **2012**, *40*, 1095–1101.
9. Sun, L.; Xin, X.T.; Ren, J.L. Road performance of nano−modified asphalt mixture. *J. Southeast Univ. Nat. Sci. Ed.* **2013**, *4*, 203–206.
10. Ye, C.; Chen, H.X.; Wang, C. Research on Road Performance of Nano−TiO_2 Modified Asphalt Mixture. *Sino Foreign Highw.* **2010**, *3*, 322–325.
11. Ye, C.; Chen, H.X. Research on Road Performance of Nano−SiO_2 and Nano−TiO_2 Modified Asphalt. *New Build. Mater.* **2009**, *36*, 82–84.
12. Yang, H.H.; Yuan, H.W.; Hao, P.W. Research on road performance of lignin fiber asphalt mixture. *Highw. Transp. Sci. Technol.* **2003**, *20*, 10–11.
13. Wu, J.R.; Qi, D.J. Effect of polyester fiber content and freeze−thaw cycle on the water stability of asphalt mixtures. *Silic. Bull.* **2017**, *4*, 311–315.
14. Zhao, Y.H.; Zhao, L.D.; Fan, Y.F.; Guo, N.S. High temperature and water stability of polyester fiber modified asphalt mixture. *J. Build. Mater.* **2008**, *5*, 51–55.

15. Liu, S. Research on Road Performance of Glass Fiber Asphalt Mixture. Master's Thesis, Chongqing Jiaotong University, Chongqing, China, 2016.
16. Li, L.Q. Application of basalt fiber in asphalt pavement of long uphill section. *J. Zhejiang Jiaotong Vocat. Tech. Coll.* **2011**, *3*, 20–22.
17. Wu, S.P.; Ye, Q.S.; Liu, Z.F. Research on mineral fiber to improve the high temperature stability of asphalt mixture. *Highw. Transp. Sci. Technol.* **2008**, *11*, 24–27.
18. Cheng, Y.; Zhu, C.; Tan, G.; Lv, Z.; Yang, J.; Ma, J. Laboratory Study on Properties of Diatomite and Basalt Fiber Compound Modified Asphalt Mastic. *Adv. Mater. Sci. Eng.* **2017**, *2017*, 1–10. [CrossRef]
19. Qin, X.; Shen, A.; Guo, Y.; Li, Z.; Lv, Z. Characterization of asphalt mastics reinforced with basalt fibers. *Constr. Build. Mater.* **2018**, *159*, 508–516. [CrossRef]
20. Wu, Z.G.; Xia, Y.; Lu, R.Y.; Lu, Y.F.; Cao, J.W. Experimental study on the performance of graded basalt fiber reinforced modified asphalt mixture. *Constr. Technol.* **2018**, *47*, 62–65 + 76.
21. Ren, G.M.; Gu, X.Y.; Tian, P. Research on fatigue performance of basalt fiber asphalt mortar. *Highw. Transp. Sci. Technol. Appl. Technol. Ed.* **2012**, *4*, 78–79.
22. Yang, J.S. Research on Road Performance and Low Temperature Characteristics of Basalt Fiber SMA−13. Master's Thesis, Jilin University, Changchun, China, 2018.
23. Wang, D.; Linbing, W.; Christian, D.; Zhou, G. Fatigue Properties of Asphalt Materials at Low In−Service Temperatures. *J. Mater. Civ. Eng.* **2013**, *25*, 1220–1227. [CrossRef]
24. Gu, X.; Xu, T.; Ni, F. Rheological Behavior of Basalt Fiber Reinforced Asphalt Mastic. *J. Wuhan Univ. Technol. Mater. Sci. Ed.* **2014**, *29*, 950–955. [CrossRef]
25. Gao, C.M. Research on the Performance of Basalt Fiber Asphalt Concrete and Microscopic Analysis of the Strengthening Mechanism. Master's Thesis, Jilin University, Changchun, China, 2012.
26. Zhang, X.Y.; Gu, X.Y.; Lv, J.X. Effect of basalt fiber distribution on the flexural−tensile Theological performance of asphalt mortar. *Constr. Build. Mater.* **2018**, *179*, 307–314. [CrossRef]
27. Zhang, X.; Gu, X.; Lv, J.; Zou, X. 3D numerical model to investigate the rheological properties of basalt fiber reinforced asphalt−like materials. *Constr. Build. Mater.* **2017**, *138*, 185–194. [CrossRef]
28. Omranian, S.R.; Hamzah, M.O.; Valentin, J.; Hasan, M.R.M. Determination of optimal mix from the standpoint of short term aging based on asphalt mixture fracture properties using response surface method. *Constr. Build. Mater.* **2018**, *179*, 35–48. [CrossRef]
29. Kim, D.H.; Jeong, E.; Oh, S.E.; Shin, H.S. Combined (alkaline + ultrasonic) pretreatment effect on sewage sludge disintegration. *Water Res.* **2010**, *44*, 3093–3100. [CrossRef]
30. Kushwaha, J.P.; Srivastava, V.C.; Mall, I.D. Organics removal from dairy waste water by electrochemical treatment and residue disposal. *Sep. Purif. Technol.* **2010**, *76*, 198–205. [CrossRef]
31. Wang, W.; Cheng, Y.; Tan, G. Design Optimization of SBS−Modified Asphalt Mixture Reinforced with Eco−Friendly Basalt Fiber Based on Response Surface Methodology. *Materials* **2018**, *11*, 1311. [CrossRef]
32. Valencia, L.E.C.; Ramirez, A.M.; Guzman, E.A.; Garcia, M.E.C. Modelling of the performance of asphalt pavement using response surface methodology−the kinetics of the aging. *Build. Environ.* **2007**, *42*, 933–999. [CrossRef]
33. Moghaddam, T.B.; Soltani, M.; Karim, M.R.; Baaj, H. Optimization of asphalt and modifier contents for polyethylene terephthalate modified asphalt mixtures using response surface methodology. *Measurement* **2015**, *74*, 159–169. [CrossRef]
34. *JTG E20−2011. Standard Test Methods of Asphalt and Asphalt Mixtures for Highway Engineering*; Ministry of Transport: Beijing, China, 2011. (In Chinese)
35. *GB/T 38111−2019. Classification, Gradation and Designation of Basalt Fiber*; National Standardization Management Committee: Beijing, China, 2019. (In Chinese)
36. *JTG E42−2005. Test Methods of Aggregate for Highway Engineering*; Ministry of Transport: Beijing, China, 2005. (In Chinese)
37. Zhang, Z.Z.; Han, C.L.; Li, C.W. Application of Response Surface Method in Experimental Design, and Optimization Application of Response Surface Method in Experimental Design and Optimization. *J. Henan Educ. Inst. Nat. Sci. Ed.* **2011**, *20*, 34–37.
38. Gong, Y.; Bi, H.; Tian, Z.; Tan, G. Pavement Performance Investigation of Nano−TiO_2/$CaCO_3$ and Basalt Fiber Composite Modified Asphalt Mixture under Freeze-Thaw Cycles. *Appl. Sci.* **2018**, *8*, 2581. [CrossRef]

39. Liu, D.L.; Yue, A.J.; Chen, L. Study on the properties of nano−calcium carbonate modified asphalt and its mixture. *J. Chang. Jiaotong Univ.* **2004**, *18*, 70–72.
40. Ni, P. Design and Road Performance Test of Basalt Fiber SMA−13 Mixture. Master's Thesis, Jilin University, Changchun, China, 2017.
41. Sun, X. Research on the properties of diatomaceous earth/basalt fiber composite modified asphalt and asphalt mixture. *New Build. Mater.* **2019**, *46*, 90–94.
42. *JTG F40−2004. Technical Specifications for Construction of Highway Asphalt Pavements*; Ministry of Transport: Beijing, China, 2004. (In Chinese)